Influence of dopants on thermal stability and densification of β-tricalcium phosphate powders

Nicolas Somers [a,c,*], Florian Jean [a,c], Marie Lasgorceix [a,c,d], Hugo Curto [a,c,e], Giovanni Urruth [f], Anthony Thuault [a,c], Fabrice Petit [b,c], Anne Leriche [a,c]

[a] *Univ. Polytechnique Hauts-de-France, EA 2443 - LMCPA - Laboratoire des Matériaux Céramiques et Procédés Associés, F-59313 Valenciennes, France*
[b] *Belgian Ceramic Research Centre – Member of EMRA, Av. Du Gouverneur E. Cornez 4, Mons B-7000, Belgium*
[c] *GIS TECHCERA – Groupement Intérêt Scientifique Transfrontalier sur Les Céramiques (BE -FR), France*
[d] *INSA Hauts-de-France, Campus Mont Houy, 59313 Valenciennes Cedex 9, France*
[e] *Sairem SAS, 82 Rue Elisée Reclus, 69150 Décines-Charpieu, France*
[f] *Marion Technologies, Parc Technologique Delta Sud, 55 Rue Louis Pasteur, 09340 Verniolle, France*

ARTICLE INFO

ABSTRACT

In this work, β-tricalcium phosphate (β-TCP) is doped with Mg^{2+} and Sr^{2+} in order to postpone the problematic β-TCP → α-TCP transition occurring from 1125 °C. Indeed, this phase transition occurs with a large lattice expansion during sintering causing microcracks and a reduced shrinkage leading to poor mechanical properties of ceramic parts. The substitution of calcium by cations like Mg^{2+} and Sr^{2+} allows to increase the temperature corresponding to β→α-TCP transition and therefore to increase the sintering temperature and achieve higher densification level. Three doping rates for each dopant individually (2.25, 4.50 and 9.00 mol%) and two co-doped compositions (2.00 mol% and 4.00 mol% of Mg^{2+} and Sr^{2+} simultaneously) were tested. Thermal and dilatometric analyses were used to evaluate the effects of Mg^{2+} and Sr^{2+} doping on the thermal stability of β-TCP. It has been shown that all doping, except the 2.25 mol% Sr-TCP, postpone the β→α transition. These results were confirmed after conventional and microwave sintering. Indeed, X-ray diffraction analyses of sintered pellets showed that the only phase present is β-TCP up to 1300 °C in all compositions except for the 2.25 mol% Sr-TCP with both sintering ways. Moreover, a higher densification rate is observed with the presence of dopants compared to undoped β-TCP according to the microstructures and relative densities close to 100%. Finally, the duration of microwave sintering is almost sixteen times shorter compared to conventional sintering allowing rapid densification with similar final relative densities and microstructures with finer grains.

1. Introduction

Calcium phosphate (CaP) ceramics are widely studied and used as raw materials for bone repair applications like bone cements, osteo-conductive coatings on metal prostheses or porous scaffolds [1–6]. Their chemical similarity to native mineral part of bone gives them excellent biocompatibility and osteoconduction properties. Indeed, they can conduct bone regrowth and facilitate cell proliferation and differentiation into osteoblasts. Moreover, CaPs are safe, easily and inexpensively produced and can be certified for clinical use [7].

Among CaPs, β-tricalcium phosphate (β-TCP, β-Ca$_3$(PO$_4$)$_2$) is one of the most attractive biomaterials for bone repair due to its interesting biological properties. Owing to its high resorption rate in human body, it is foreseen to be used as temporary support for natural tissue colonization in surgical and dental applications. Typically, β-TCP bone substitutes are suitable to heal bone defects and fill bone voids generated by surgeries or diseases. After implantation, β-TCP is gradually resorbed and replaced by newly formed bone within 6–24 months [4,8–12]. This bioresorption makes β-TCP particularly interesting compared to other calcium phosphate like hydroxyapatite $Ca_{10}(PO_4)_6(OH)_2$ (HA). Indeed, the lack of degradation of HA bone substitutes can lead to bone deformities and a risk of bone fracture around the implant [5].

β-TCP is already used to produce powders, granules, dense blocks, injectable formulations or self-setting cements for bone filling. In

addition, porous scaffolds seem very promising because their structures allow cells and extracellular matrices interaction while providing the mechanical support for growing cells and tissue. Indeed, the presence of porosity provides higher surface area improving interactions between the implant and the biological environment [4,13]. Nevertheless, there are still some issues for β-TCP macroporous scaffolds fabrication. In fact, β-TCP cannot be used as scaffolds in large bone defects or in load-bearing areas due to its weak mechanical properties, especially brittleness and hardness [14–20]. The major drawback in the manufacturing of these scaffolds is the difficulty to densify the β-TCP at high temperatures. Indeed, the tricalcium phosphate presents an allotropic phase transition from the rhomboedric β phase to the monoclinic α-TCP from 1125 °C [5,21,22]. The temperature of this transition highly depends on the purity of the powder as well as the preparation conditions and can vary over a very broad range of temperature (from 1120 °C to 1200 °C) in the presence of elemental impurities [14,20,23]. The phase transition occurs with a large lattice expansion (about 7%) during sintering causing microcracks and a reduced shrinkage [14,23–26]. In addition to these physical issues, the β→α transition also generates an increase of the solubility in biological media leading to a too fast and uncontrolled resorption of the TCP bone substitute [27,28].

Currently, two solutions are considered and studied to reach high densification (>99% relative density) of β-TCP parts. The first option is the possibility to introduce sintering additives like hydroxyapatite [20] or dopants [29,30] in the β-TCP structure to increase its thermal stability allowing a higher temperature treatment [31–34]. In addition, dopants have been proven to increase the sintered relative density up to 5% [35] and enhance the compressive strength [32,35]. There are many examples of studies using dopants, mostly cations like Mg^{2+}, Sr^{2+}, Cu^{2+}, Si^{4+}, Zn^{2+}, or Ag^+, incorporated inside the β-TCP structure [9,14,23,31–33, 36–50]. Most of the time, doping aims to improve biological properties like osteoconductive or antibacterial behaviour. However, dopants can also bring a beneficial effect on the β phase stability. These dopants are able to substitute the Ca^{2+} into the β-TCP lattice and change the strength of chemical bonds and lattice parameters [23,49,51]. For some Ca-substitutional ions like magnesium or strontium, it leads to the β→α transition postponement upon heating, thus increasing the β phase stability field [14,23,24,31,33] and the TCP sinterability. Indeed, in addition to stabilizing the beta phase, higher densification can occur in the presence of dopants like strontium due to an increase of ion diffusion during sintering [52].

The second solution for an improved densification of β-TCP could be the use of alternative densification processes like Spark Plasma Sintering (SPS) [53], hot pressing [54] or microwave sintering [32,55–57]. According to Champion [22], the use of pressure-assisted sintering can lead to full densification (>99%) of β-TCP without additives at a temperature below the β-TCP → α-TCP transition and its issues. Field assisted sintering like microwave sintering can be employed to densify faster the material as well as obtain controlled and finer microstructures leading to higher mechanical properties [32,55–57]. Moreover, several recent researches tend to combine additive manufacturing techniques with rapid sintering processes in order to quickly produce ceramic bone substitutes scaffolds [55,57,58]. Indeed, the on-demand bone scaffold fabrication for patient bone surgeries is limited by the long and complex sintering processes needed to consolidate the scaffolds [57]. The sintering becomes the time-limiting step losing the benefits of some fast additive manufacturing methods.

As the field of application, in which this work fits, concerns the production of macroporous scaffolds with complex shapes as well as fine and dense walls for which pressureless sintering is more suitable. For this reason, the combination of sintering additives like dopants and microwave sintering could be a strong tool to manufacture dense customized biomaterials in a few hours. In addition to that, volumetric heating via microwave radiation ensures uniform heating with almost no thermal gradient. This allows higher heating rates, reduces the processing time, and enables limited grain growth [55,56]. The control of

the grain size can be interesting due to its well-known influence on the mechanical properties. Indeed, smaller grain size generally leads to improved fracture toughness and hardness [18,53,59–61].

Despite its benefits, microwave sintering devices usually does not allow a very precise control of the temperature using most of the time pyrometers to get the sample surface temperature [56,58,62]. This lack of temperature control can be critical with β-TCP and its phase transition to α-TCP at quite low temperature. In addition to that, the direct interaction of microwaves with the sample and the sudden variation in dielectric losses can lead to thermal runaway [63].

In this context, this work aims to produce doped β-TCP powders with improved thermal stability allowing higher sintering temperature and therefore higher level of densification. Doped β-TCP powders were produced by aqueous precipitation to optimize reagent mixing and avoid solid route issues. Indeed, solid route synthesis involves a difficult control of the reagents mixing and the completeness of the reaction between them can lead to a variability in the composition of the final powder [2]. In parallel to doped powders characterizations, conventional and microwave sintering (MW) were tested at temperatures under and above the usual phase transition temperature of β-TCP to assess their thermal behaviour during densification. The two sintering processes are compared in terms of phase composition, densification and microstructure. In order to do that, doped powders were shaped after the synthesis by mold casting and then sintered.

Magnesium and strontium were chosen for this study where several doping rates of each dopant were tested as well as co-doping to combine benefits of both cations. On one hand, magnesium is known to have an essential role in human physiology and to improve the biocompatibility of implants [24]. Then, it presents the most valuable results in terms of β-TCP stabilization [23,24,32]. On the other hand, strontium can enhance bone regeneration in synthetic bone grafts and is used for treatment of osteoporosis [32,33]. Moreover, Tarafder et al. [32] have shown that the addition of SrO and MgO dopants in TCP results in smaller grain size, increased density and pore size reduction that could be beneficial for the mechanical properties of sintered parts. To author's knowledge, only Bose et al. [31,32,47,64] and Kannan et al. [65] studied the combination of these two cations. These works showed a good potential from a mechanical and biological point of view for Mg–Sr co-doped TCP. Indeed, the presence of SrO and MgO in TCP on early wound healing was clearly exhibited by increased osteoid and bone formation as compared with undoped TCP. They also revealed faster bone formation in rats with doped β-TCP implant compared to rats with pure β-TCP implant.

Bose et al. [31,32,47,66] studied the doping of TCP by solid route synthesis from a commercial β-TCP powder. So, there is a lack of knowledge concerning the doping by aqueous precipitation which could be very interesting to tailor the powder properties in function of the desired application. Moreover, the effect of dopants on the thermal stability was not deeply assessed. Kannan et al. [65] did study the Mg^{2+} and Sr^{2+} doping of TCP by aqueous precipitation from a structural point of view with the help of Rietveld refinement. However, there is still a lack of knowledge about the thermal behaviour of such doping and the influence on the sintering of such co-doped compositions. Finally, the use of microwave heating is a very promising fast sintering process for potential implant ceramics. The capacity of densification with limitation of grain growth as well as unified linear and volumetric shrinkage can improve mechanical strength of bioceramics and extend their applications [32,67]. Few researches have studied the combination of doping and microwave sintering with β-TCP as well as CaP in general [32,52, 67–69].

That is why, the main purpose of this article is to study deeper the effect of Mg and Sr doping on the thermal stability and both conventional and microwave sintering of TCP. Thermal analysis and dilatometry are a strong tool to characterize these as showed by Frasnelli et al. [14] and Enderle et al. [23]. The use of these techniques as well as physico-chemical characterizations allow a complete study of the TCP
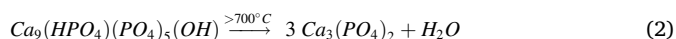
doping by Sr and Mg.

In order to reach this objective, three doping amounts were tested for each dopant individually (2.25, 4.50 and 9.00 mol%). These doping amounts were chosen according to the works of Enderle et al. [23] and Frasnelli et al. [14] on the influence of Mg^{2+} doping in $Ca_3(PO_4)_2$. These authors showed that the maximum thermal stability of Mg-TCP is reached with a doping amount of 9.1 mol%. The two other doping amounts, 2.25 and 4.50 mol%, were chosen to have a complete comparison of the dopant amount. The same strategy was applied for the Sr^{2+} doping to study the effect of the dopant nature on β-TCP properties. Indeed, it is already known that strontium has a smaller effect on the β-TCP stabilization but, to authors knowledge, there is no clear comparison available between these two dopants for the same doping amounts [32,33,70,71]. Moreover, two co-doped compositions were also studied: 2.00 and 4.00 mol% of both dopants simultaneously to combine benefits of Mg^{2+} and Sr^{2+}.
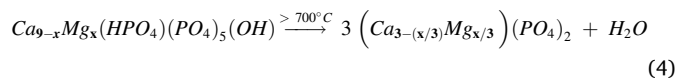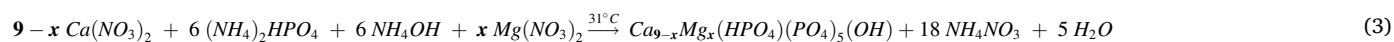
2. Experimental

2.1. Doped β-TCP powder synthesis

β-TCP powders were produced in two main steps: i) the synthesis of an apatitic tricalcium phosphate, $Ca_9(HPO_4)(PO_4)_5OH$ which is the precursor of β-TCP and is prepared by aqueous precipitation technique using a diammonium phosphate solution $(NH_4)_2HPO_4$ (98.0–102.0%, Carlo Erba, France) and a calcium nitrate solution $Ca(NO_3)_2.4H_2O$ (>98.0%, Honeywell, Germany) inside a double-wall reactor. Typically, the diammonium phosphate solution was added to the calcium nitrate solution by controlling addition speed, pH and temperature. The mixture pH was adjusted to a constant value of 6.7 by a continuous addition of ammonium hydroxide while temperature was fixed to 31 °C. The apatitic tricalcium phosphate precipitate was extracted, filtered and dried after a ripening time of 20 h. After drying, a further calcination (850 °C, 3 h) was needed to remove residual reaction by-products like ammonium nitrate, to induce a decrease of the specific surface of the raw powder and mainly to transform the amorphous apatitic precursor into the final, stable and crystallized β-TCP [2,20,72]. These synthesis steps are reported in the following equations (1) and (2):

$$9\ Ca(NO_3)_2 + 6\ (NH_4)_2HPO_4 + 6\ NH_4OH \xrightarrow{31°C} Ca_9(HPO_4)(PO_4)_5(OH) + 18\ NH_4NO_3 + 5\ H_2O \tag{1}$$

$$Ca_9(HPO_4)(PO_4)_5(OH) \xrightarrow{> 700°C} 3\ Ca_3(PO_4)_2 + H_2O \tag{2}$$

Doped β-TCP powders were produced by adding magnesium and/or strontium cations as nitrates, $Mg(NO_3)_2$ (98.0–102.0%, MW 256.41, Alfa Aesar, Germany) and $Sr(NO_3)_2$ (>99%, MW 211.63, Carlo Erba, France), into the calcium nitrate solution. The stoichiometric amount of calcium was reduced to allow dopant substitutions but the ratio (Ca + dopant)/P was kept at 1.5 corresponding to stoichiometric β-TCP. Indeed, the objective is to synthesize pure doped β-TCP powders without any other CaP phases like hydroxyapatite $(Ca_{10}(PO_4)_6(OH)_2$, HA) or calcium pyrophosphate $(Ca_2P_2O_7$, CPP). The synthesis of Mg-doped β-TCP is reported as example in the following equations (3) and (4):

$$\boldsymbol{9-x}\ Ca(NO_3)_2 + 6\ (NH_4)_2HPO_4 + 6\ NH_4OH + \boldsymbol{x}\ Mg(NO_3)_2 \xrightarrow{31°C} Ca_{\boldsymbol{9-x}}Mg_{\boldsymbol{x}}(HPO_4)(PO_4)_5(OH) + 18\ NH_4NO_3 + 5\ H_2O \tag{3}$$

$$Ca_{\boldsymbol{9-x}}Mg_{\boldsymbol{x}}(HPO_4)(PO_4)_5(OH) \xrightarrow{> 700°C} 3\left(Ca_{\boldsymbol{3-(x/3)}}Mg_{\boldsymbol{x/3}}\right)(PO_4)_2 + H_2O \tag{4}$$

Three doping amounts were tested for each dopant individually (2.25, 4.50 and 9.00 mol%) and two co-doped compositions (2.00 and 4.00 mol% of both dopants simultaneously).

2.2. Shaping of doped β-TCP powders

After calcination at 850 °C for 3 h, powders were ball milled during 4 h (90 g of powder for 200 g of water) in a high-density polyethylene (HDPE) milling jar with 1 kg of partially stabilized zirconia (Y-PSZ) grinding media (balls with 10, 15, 20 mm diameter in 25, 50 and 25 wt% proportion respectively). This milling allows to reduce the aggregate size down to around 2 μm by breaking up agglomerates formed during the calcination. The milling step is also necessary to obtain optimal powder characteristics in order to shape them into pellets.

The milled powders were then dried and shaped to pellets by mold casting. β-TCP slurries were prepared with a fixed powder concentration of 65 wt% in water with a commercial organic defloculant (Darvan C,R. t.Vanderbilt. Co.) introduced in amount 0.002 g m^{-2} with respect to the powder surface area. After an hour of ball milling using HDPE milling jar and Y-PSZ grinding media, slurries were poured into cylindrical plastic molds with 14 mm diameter and 10 mm height. Pellets were dried at room temperature during 24 h before sintering.

2.3. Sintering of doped β-TCP pellets: conventional and microwave routes

Pellets of each powder (undoped and doped β-TCP) were sintered by MW and by conventional heating in an electric furnace.

On one hand, conventional sintering was carried out with a ramp rate of 5 °C·min^{-1} to sintering temperature (ranging from 1100 °C to 1300 °C) with a 3 h dwell time.

On the other hand, microwave sintering was performed in a cuboid resonant single-mode cavity at 2.45 GHz (Sairem). This set-up is described by Thuault et al. [73]. The surface temperature of the samples was read by a pyrometer (Modline® 5, Ircon). Samples were placed into an insulating box made of alumina-silica fibres (Unifrax, Fiferfrax Duraboard 1600) and sintered by microwave hybrid heating. To do so, a silicon carbide ring susceptor was used to initiate the radiative heating at room temperature and reach a sufficient temperature allowing a β-TCP dielectric loss necessary to microwave heating of the samples. Sintering temperatures were set at 1100, 1200 and 1300 °C with a dwell time of 10 min. Heating and cooling rate during MW sintering were about 100 °C·min^{-1}.

2.4. Characterization techniques

2.4.1. Physico-chemical characterization of the powders

Purity of the raw material was assessed on powders calcined at 1000 °C for 15 h just after drying according to the standard procedure
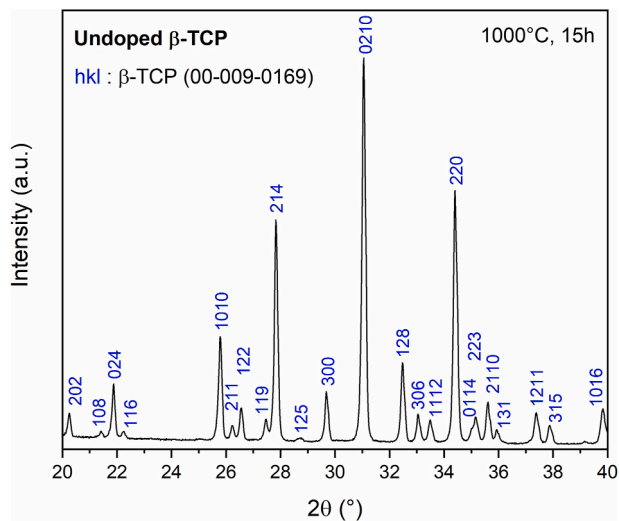
Fig. 1. XRD pattern of undoped β-TCP powder treated 1000 °C during 15 h (2Θ range: 20–40°).
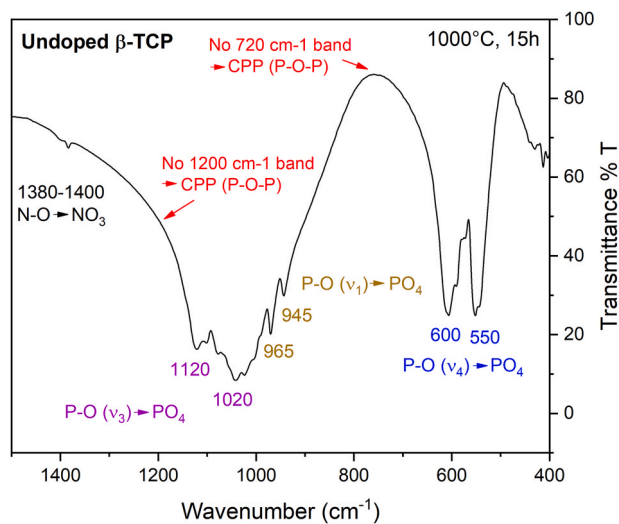

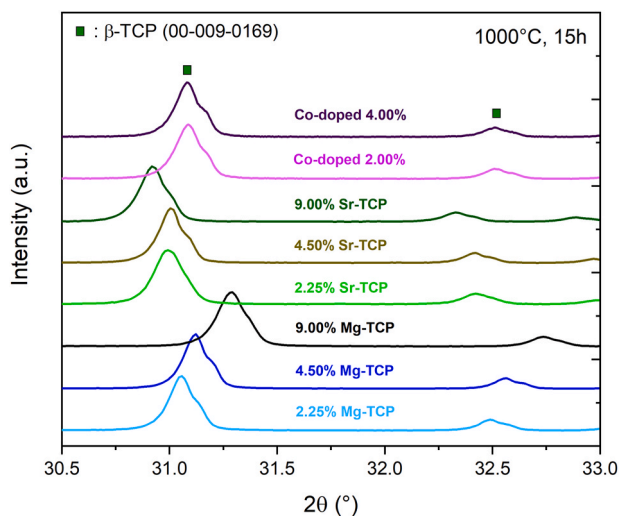**Fig. 2.** IR spectrum of undoped β-TCP powder (1000 °C, 15 h).

Fig. 3. XRD patterns of doped and co-doped β-TCP powders (1000 °C, 15 h).

NF ISO 13779–3:2008–04. infrared spectroscopy (IR). The detection of HA phase was performed by powders X-ray diffraction (XRD) with the HA (211) (2θ = 31.772°) most intense diffraction peak. The presence of HA as a secondary phase in β-TCP can be detected down to 0.5 wt% from XRD [6]. Concerning the CPP phase, its most intense XRD useable peak (202) (2θ = 28.9°) is only observable for quantities greater than 4 wt%. Thus, the detection of CPP was verified by infrared spectroscopy (IR) with its 720 cm^{-1} and 1200 cm^{-1} characteristic bands. Indeed, the presence of CPP is already visible from 1 wt% with IR [2,20].

XRD patterns were recorded using a θ/2θ diffractometer (Panalytical X'PERT PRO) working with Cu Kα radiation (1.541874 Å) at 45 kV and 40 mA; the measurement was carried out in the 2θ range of 10–60°, with step of 0.0066° and 78.795 s of acquisition time. The crystalline phases were identified using Joint Committee on Powder Diffraction-International Centre for Diffraction Data (JCPDS-ICDD) files. In addition, Rietveld refinement using the Profex software [74] was used to determine lattice parameters of the different compositions as well as for the quantification of potential other phases like HA and CPP using their corresponding structure files. XRD measurements were also carried out on the surface of sintered pellets to investigate the presence of α-TCP. All the diffractograms were normalized with the most intense peak (31.027° (0210)) of the β-TCP phase fixed at 100.

Infrared spectra of powders were recorded on a Fourier transform spectrometer (Jasco-FT/IR-460 Plus) in the 4000–400 cm^{-1} region with a resolution of 2 cm^{-1}.

The purity and chemical composition of the synthesized powders were checked by inductivity coupled plasma – atomic emission spectroscopy (ICP-AES, ICP-AES, Shimadzu ICPE-9820, 125–770 nm) using ultrapure standards (SCP Science PlasmaCAL). Standards and samples were dissolved in ultrapure nitric acid (70 vol%) and diluted in pure water (1, 20, 30 and 50 mg/L). ICP-AES measurements allow to determine the dopant (s)/(Ca + dopant(s)) molar ratios as well as the (Ca + dopant(s))/P ratios.

2.5. Thermal stability of doped and co-doped β-TCP

In order to assess the thermal behaviour of the produced powders, Differential Thermal Analysis (DTA) and Thermogravimetric Analysis (TGA) experiments were carried out using a LabSysEvo (Setaram) equipment on uncalcined and dried powders with sample weight about 25 mg, heating rate 10 °C·min^{-1} from 20 to 1500 °C, air flow 40 mL min^{-1}. TGA gives useful information about water loss, decomposition of by-products or other reactions. On the other side, DTA helps to determine at which temperature the ATP is converted into β-TCP and the β→α transition temperature.

2.6. Sintering of doped and co-doped β-TCP

In the interest of studying the thermal stability of the different doped compositions during densification, dilatometric analyses were carried out on casted parallelepiped shaped pellets using a Dil-402 C (Netzsch) dilatometer. Before analyses, pellets were pre-sintered at 1000 °C for 12 h to observe the interruption of shrinkage associated with the α-TCP formation. This pre-sintering step is necessary to eliminate the shrinkage due to the densification of the sample. If not, the shrinkage due to the β -> α transformation cannot be detected with the experimental device. Thermal expansion-shrinkage of these pellets was measured in air atmosphere. Measurements were performed with a 5 °C·min^{-1} heating rate up to 1500 °C and 5 °C·min^{-1} cooling.

Relative densities (RD) of sintered pellets were determined by the Archimedes' method in deionized water at room temperature. The weighing process was conducted on an analytical balance with a resolution of 0.1 mg. A series of 3 samples per composition and temperature were analyzed to obtain average relative density values. Theoretical densities were obtained by Rietveld refinement of diffractograms obtained for each composition (Profex). The microstructures were observed on pellet surfaces using scanning electron microscopy (SEM,
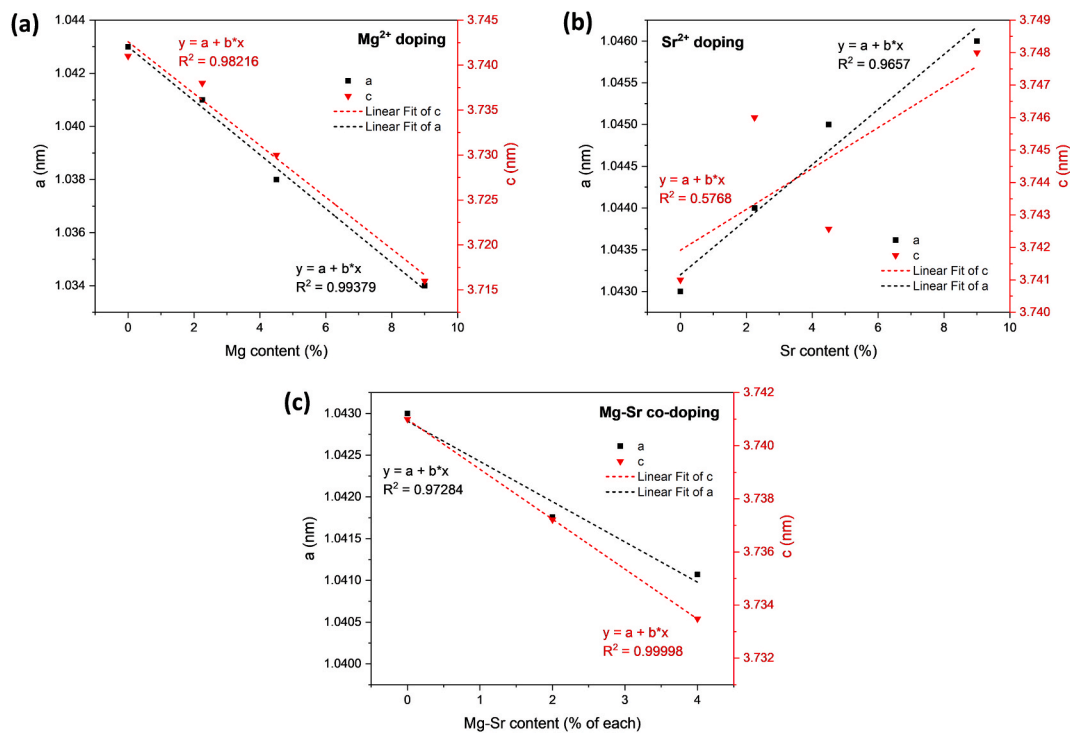
Fig. 4. Lattice parameters (a-axis and c-axis) for the different compositions obtained by Rietveld refinement (Profex).

Table 1

Comparison between experimental lattice parameters and results obtained by other research groups [1]. P.M.C. Torres et al., 2016 [2] Enderle et al., 2005 [3] Boanini et al., 2019 [4] Kanna et al., 2009.

Powders	a-axis (nm)		c-axis (nm)	
	Experimental	Literature	Experimental	Literature
Undoped	1.043	1.044 [1–3]	3.741	3.739 [1–3]
2.25% Mg	1.041	2.00% Mg: 1.041 [1]	3.738	3.736 [1]
4.50% Mg	1.038	4.00% Mg: 1.039 [2]	3.730	4.00% Mg: 3.731 [2]
9.00% Mg	1.034	8.00% Mg: 1.035 [2]	3.716	8.00% Mg: 3.717 [2]
2.25% Sr	1.044	2.00% Sr: 1.044 [3]	3.746	2.00% Sr: 3.739 [3]
4.50% Sr	1.045	5.00% Sr: 1.045 [3]	3.741	5.00% Sr: 3.739 [3]
9.00% Sr	1.046	10.00% Sr: 1.046 [3]	3.748	10.00% Sr: 3.742 [3]
2.00–2.00% Mg–Sr	1.040	1.042 [4]	3.733	3.737 [4]
4.00–4.00% Mg–Sr	1.041	1.041 [4]	3.732	3.732 [4]

Hitachi SU5000, BSE 15.0 kV ×5.00 k) after polishing and thermal etching. The polishing was carried out using SiC paper discs and diamond pastes (down to 0.5–3 μm) and the samples were put at 950 °C for 15 min (Nabertherm N 7H 1280 °C) for the thermal etching. Grain size measurements were carried out by image treatment (*Image J*) on 60 grains with 4 measurements by grain. The average grain sizes were multiplied by $4/\pi$ according the Abercrombie relation to get the radius of a particle from any profile [75].

3. Results and discussions

3.1. Synthesis of undoped β-TCP

Fig. 1 shows the XRD pattern of undoped β-TCP powder (1000 °C, 15

h). The diffractogram is the typical diffraction pattern of β-TCP with the absence of secondary phase like HA or CPP. The infrared analysis of undoped β-TCP powder (1000 °C, 15 h) is visible on Fig. 2 with the description of the main characteristic bands of β-TCP. No trace of CPP is found in the corresponding IR spectrum confirming the synthesis of pure undoped β-TCP. This undoped β-TCP powder is used as a reference for studying thermal behaviour.

3.2. Synthesis of doped β-TCP powders

As shown in Fig. 3, XRD patterns of Mg- and Sr-doped and co-doped β-TCP powders are characterized by the absence of HA as well as CPP and all diffraction peaks correspond to the β-TCP phase. Rietveld refinements indicate the presence of 100% of β-TCP without HA or CPP. Moreover, small shift in peak positions was observed for doped samples compared to undoped β-TCP. Fig. 4 shows changes in lattice parameters for the different compositions. Typically, a linear Vegard's law is observed for the different cation doping [76]. A comparaison with lattice parameters obtained by other research groups is made in Table 1. The experimental data are generally consistent with those of the literature. Fig. 5 represents the crystal structure of β-TCP and its different crystallographic sites to support the discussion.

According to Enderle et al. [23], Mg^{2+} can only replace Ca^{2+} on Ca (4) and Ca(5) sites in the β-TCP structure with a preference for Ca(5) sites (Fig. 5). This substitution of Ca^{2+} by Mg^{2+} leads to a decrease in the unit cell parameters of β-TCP structure and thus to a shift of diffraction peaks to higher 2θ values. This is due to the smaller ionic radius of Mg^{2+} (0.89 Å) compared to Ca^{2+} (1.12 Å) reducing the unit cell size [65]. Thus, the chemical bonds are shorter with magnesium. The lattice contraction caused by the Mg^{2+} substitution increases the stability of the β phase and postpones the β→α transition [32].

On the other hand, the larger ionic radius of Sr^{2+} (1.25 Å) compared to Ca^{2+} (1.12 Å) causes the opposite effect [65]. In addition, the higher the doping amount, the more marked this effect. For the Sr^{2+} incorporation, a discontinuity in the evolution of the c-axis parameters is observed. This may be due to a change of incorporation site for the strontium. Indeed, Renaudin et al. [33] suggest that strontium at doping
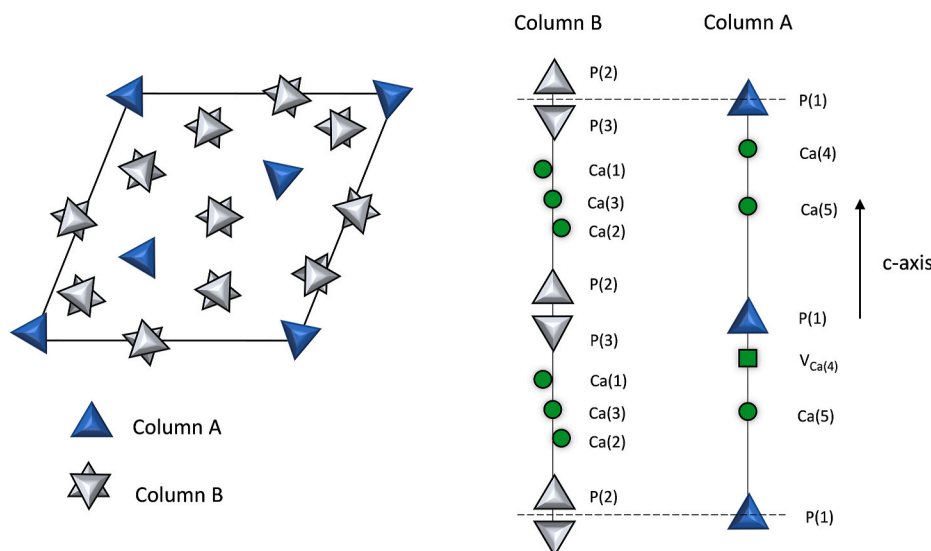
Fig. 5. Representation of the crystal structure of β-TCP from the point of view of the c axis and along the c axis (modified from Yoshida et al., 2006 [45]).
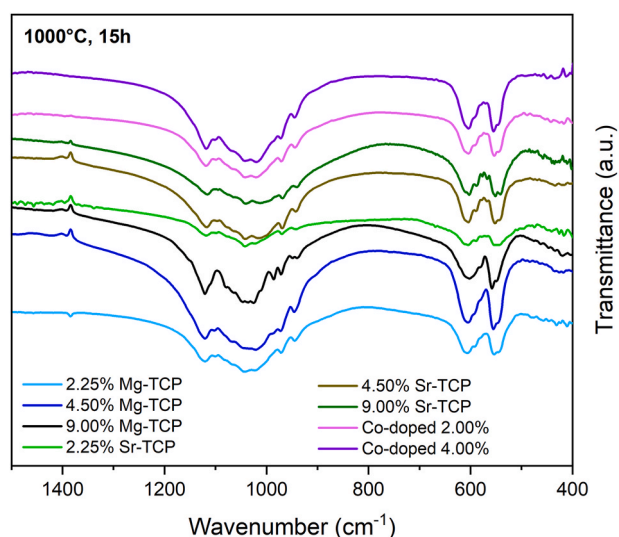

Fig. 6. IR spectra of doped and co-doped β-TCP powders (1000 °C, 15 h).

Table 2
Chemical composition of the synthesized powders obtained by ICP-AES. The values are given with a relative error of 0.01%.

Powders	Nominal Dopant(s)/(Ca + dopant(s)) (percentage)	ICP Dopant(s)/(Ca + dopant(s)) (percentage)	Nominal (Ca + dopant (s))/P (molar ratio)	ICP (Ca + dopant (s))/P (molar ratio)
Undoped		/	1.50	1.56
2.25% Mg	2.25	2.43	1.50	1.57
4.50% Mg	4.50	4.65	1.50	1.55
9.00% Mg	9,00	8.34	1.50	1.55
2.25% Sr	2.25	2.07	1.50	1.56
4.50% Sr	4.50	4.00	1.50	1.55
9.00% Sr	9.00	8.52	1.50	1.58
2.00–2.00% Mg–Sr	2.00 per each dopant	Mg: 2.80/Sr: 2.00	1.50	1.57
4.00–4.00% Mg–Sr	4.00 per each dopant	Mg: 3.93/Sr: 3.66	1.50	1.58

rates less than 5 at.% would preferentially be substituted at the Ca(4) site of β-TCP. This is also confirmed by Boanini et al. [77] through powder fitting refinements that indicates a Sr^{2+} substitution starting from Ca(4) followed by Ca(3). As the overall substitution degree increases, the filling of sites Ca(1) and Ca(2) becomes also important but the location of strontium in site Ca(5) is strongly unfavorable due to too short Ca(5)-O distances [77]. So, the discontinuity in the evolution of the c-axis parameters probably comes from the change of substitution site of Sr^{2+} with the increasing doping amount. At first strontium enters into Ca(4), causing a significant expansion of c-axis. Further strontium substitution for calcium would lead to a filling of Ca(3) sites to compensate the increment along the c-axis (Fig. 5). Finally, at higher doping rates, Sr^{2+} would continue to replace Ca^{2+} and increase the lattice size.

Finally, for the two co-dopings, the effect is like Mg-doping with a global decrease of the unit cell parameters and a shift to higher 2θ values for the diffraction peaks compared to undoped TCP. These results are consistent with the works of Banerjee et al. [31] and Kannan et al. [65]. Indeed, the last cited authors observed that the combined substitution of Sr^{2+} and Mg^{2+} with equal concentrations in the β-TCP structure caused a reduction in the unit cell parameters. This trend is due to the fact that the average size (1.07 Å) of substituted Sr^{2+} (1.25 Å) and Mg^{2+} (0.89 Å) ions, is lower than the size of Ca^{2+} ion that has been substituted (1.12 Å) [65]. This decrease of ionic radius is confirmed by the decrease of lattice parameters observed in Fig. 4 (c) for the co-doped compositions and it is consistent with the previous work of Kannan et al. [65]. Concerning the substitution sites of Mg^{2+} and Sr^{2+} in these co-doped compositions, Kannan et al. [65] also clearly show that Mg^{2+} preferably occupies the Ca(5) site of β-TCP while Sr^{2+} is easily accommodated at the Ca(4) site. So, the co-substitution of Sr^{2+} and Mg^{2+} is complementary in terms of substitution site leading to a significant reduction of the lattice size. Moreover, the incorporation of Mg^{2+} seems to play a major role in the lattice size reduction compared to Sr^{2+} [65]. That could explain the differences in the lattice parameters evolution between the Sr^{2+} (Fig. 4 (b)) and the co-doping (Fig. 4 (c)).

The IR analyses of doped and co-doped compositions are shown in Fig. 6. In the same way as the undoped β-TCP, all the infrared bands correspond to β-TCP with the visible absence of CPP characteristic bands (720 and 1200 cm^{-1}). Thus, based on XRD and IR results, this synthesis process allows to obtain doped β-TCP powders without any secondary phase.

The ICP-AES results are shown in Table 2. The dopant(s)/(Ca + dopant(s)) molar ratios show little differences with respect to the
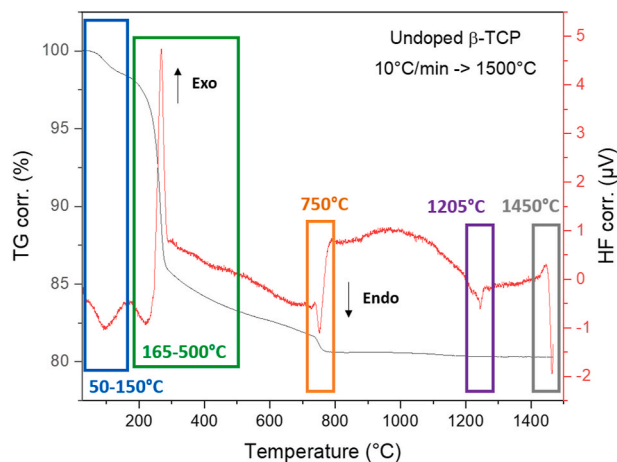
Fig. 7. Dilatometric curves of doped and co-doped β-TCP pellets (1500 °C, 5 °C·min⁻¹ heating and cooling): (a) Co-doping 4.00 mol% and 2.00, 4.50, 9.00 mol% Sr-TCP; (b) Undoped β-TCP, co-doping 2.00 mol% and 2.25, 4.50, 9.00 mol% Mg-TCP. Black dots represent the β-α transition.
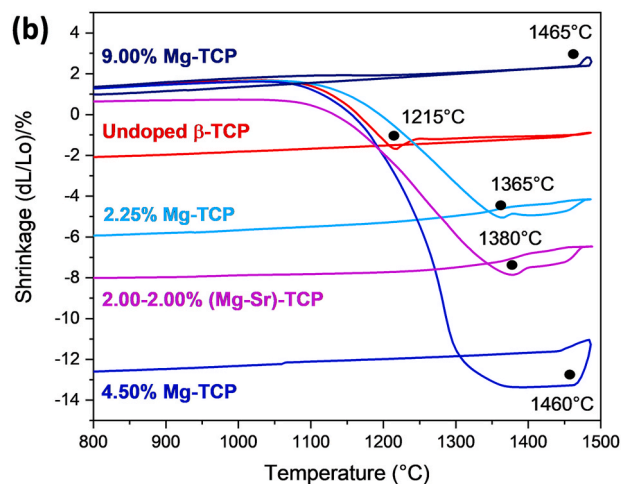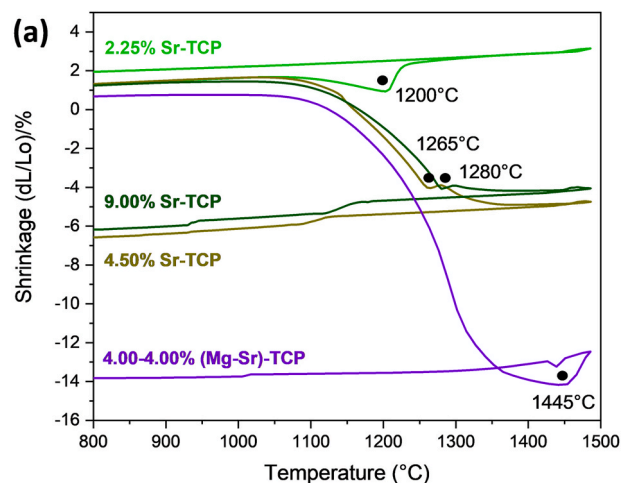

Fig. 8. TGA and DTA (TG = Thermogravimetry and HF = Heat Flow) curves of undoped β-TCP powder. TG and HF are corrected regarding the blank (alumina crucible).

Fig. 9. DTA curves of doped and co-doped β-TCP powders: (a) Co-doping 2.00 mol% and 2.25, 4.50, 9.00 mol% Mg-TCP; (b) Co-doping 4.00 mol% and 2.25, 4.50, 9.00 mol% Sr-TCP. Black dots represent the β-α transition.
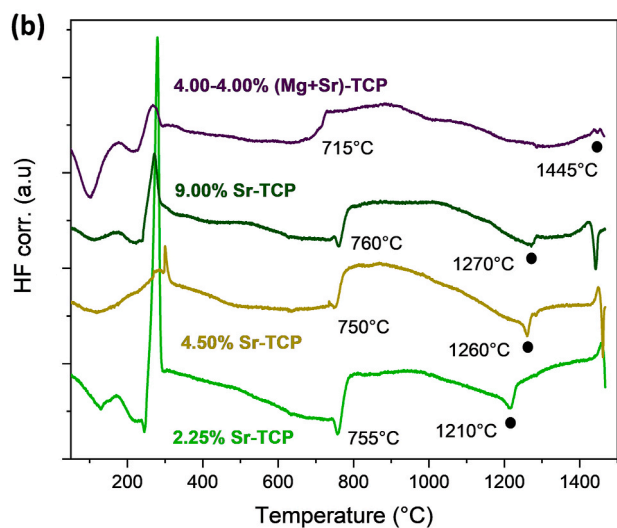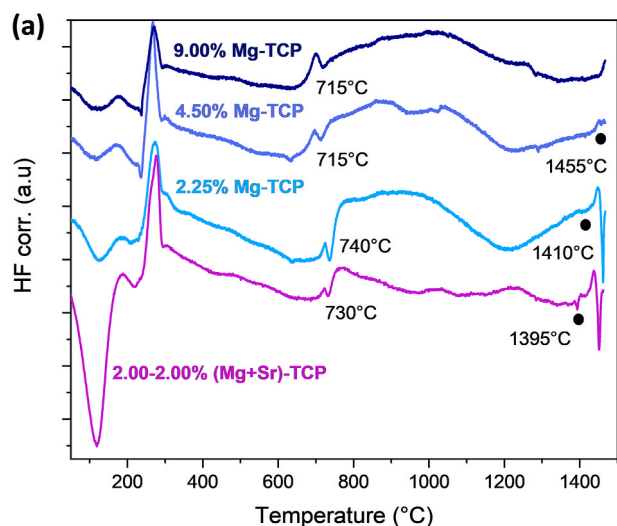
Table 3

β→ α transition temperatures observed with dilatometric and DTA experiments compared with data from the literature (Enderle et al., 2005; Frasnelli & Sglavo, 2016). Values are taken at the top of the different peaks. Temperature values from the litterature with * were measured with XRD while the other ones with DTA.

Powders	Dilatometry: β→α (T°C)	DTA: β→α (T°C)	Frasnelli et al., 2016 (T°C)	Enderle et al., 2005 (T°C)
Undoped	≈1215	≈1220	1225	1150 ± 25 °C
2.25% Mg	≈1365	≈1360	For 2.00% Mg²⁺: 1332	For 2.00% Mg²⁺: 1290 ± 25
4.50% Mg	≈1460	≈1455	For 4.60% Mg²⁺: 1474	For 4.00% Mg²⁺: 1460* ± 20
9.00% Mg	≈1465	Not detected	Not detected	For 8.00% Mg²⁺: 1540* ± 20
2.25% Sr	≈1200	≈1210	/	/
4.50% Sr	≈1265	≈1260	/	/
9.00% Sr	≈1280	≈1270	/	/
2.00–2.00% Mg–Sr	≈1380	≈1395	/	/
4.00–4.00% Mg–Sr	≈1445	≈1445	/	/

(a) Conventional sintering
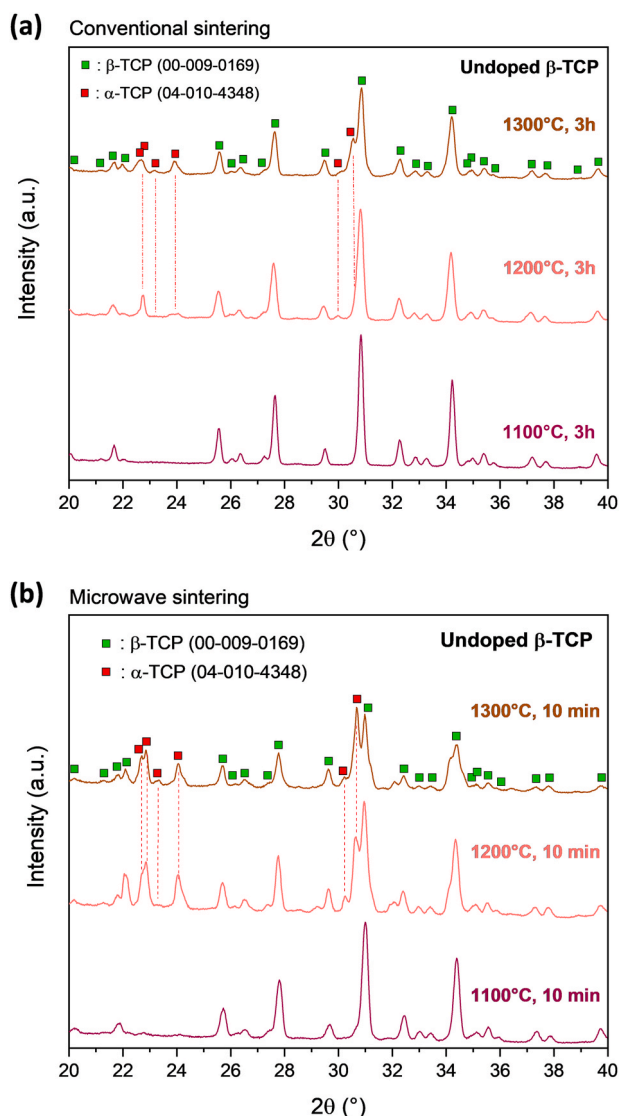

(b) Microwave sintering

Fig. 10. XRD patterns of conventionally sintered undoped β-TCP pellets at 1100, 1200 and 1300 °C for (a) conventional sintering and (b) microwave sintering.

nominal ones, probably due to the purity of the starting reagents or weighing errors. These ratios are slightly smaller than the nominal ones except in three compositions (2.25 mol% and the 4.50 mol% Mg-TCP as well as in the 2.00 mol% co-doping) where the ratios are slightly higher. Similarly, (Ca + Mg)/P atomic ratios are slightly larger than the stoichiometric 1.5 value for all the compositions probably due also to the purity of the raw materials or weighing errors. Le Gars Santoni et al. [78] showed that the purity of the final TCP powder is highly influenced by the purity of the raw materials by testing raw materials with varying purity. Therefore, the purity of the $(NH_4)_2HPO_4$ and $Ca(NO_3)_2.4H_2O$ powders could be improved to limit these differences between the nominal and the measured atomic ratios.

The shift of the XRD peaks and the changes in lattice parameters as well as the consistent ICP results confirm that the dopants have entered the β-TCP structure as predicted. Therefore, eight different compositions of pure doped and co-doped β-TCP powders are available for further treatments and comparisons with undoped β-TCP.

3.3. Thermal stability study of undoped and doped β-TCP

The thermal stabilization capacity of different amounts of dopant

was investigated by thermal analysis. TGA and DTA curves of the undoped β-TCP powder are represented in Fig. 7. The first weight loss of around 2% between 50 and 150 °C is due to residual water evaporation. Between 165 and 500 °C, the highest weight loss (about 15%) takes place and is associated with synthesis residues like ammonium nitrates or ammonia. Then, there is a continuous weight loss up to around 750 °C corresponding to the condensation of hydrogenophosphate ions before the decomposition of the ATP as explained by Destainville et al. [2] based on the works of Mortier et al. [79]. At 750 °C, the transformation of apatitic species into β-TCP takes place with a slight weight loss (about 1%) and an endothermic peak. At higher temperatures, two endothermic peaks are visible: a weak signal around 1220 °C and a strong and sharp peak around 1460 °C. The first one can be attributed to the β-TCP→α-TCP transition while the second one is associated with the α-TCP→α′-TCP transition [2,14,80]. α′-TCP is the high temperature phase stable above 1460 °C.

DTA curves of doped and co-doped β-TCP powders are shown in Fig. 8. A decrease in the formation temperature of β-TCP from the ATP is observed for the magnesium incorporation. Indeed, this transformation occurs at nearly 715 °C (4.50 and 9.00 mol% Mg^{2+}) and 735 °C (2.25 mol% Mg^{2+}) instead of 750 °C for undoped β-TCP. Thus, it is clear that the magnesium incorporation has an effect on the formation of β-TCP. This result is consistent with the work of Cacciotti et al. [80] who showed that the presence of magnesium in the calcium phosphate lattice alters the formation of β-TCP from apatite species to slightly lower temperatures. Indeed, the lattice contraction caused by the Mg^{2+} substitution tends to accelerate this multistep reaction leading to an enlargement of the β-TCP stability zone. A small peak around 1280 °C with a strong endothermic effect is visible in some DTA curves (4.50 and 9.00 mol% Mg^{2+} as well in the 4.00 mol% co-doping (Fig. 8 (a) and (b)). This peak is associated with the appearance of a liquid phase within the TCP - CPP system caused by the fusion of CPP [2]. CPP can be detected with DTA curves in CaP powders containing more than 0.5 wt% of CPP [2]. Therefore, small amounts of CPP can be present in some powders despite the absence of its characteristic bands in IR spectra where the detection limit is 1 wt% (Fig. 6).

The effect of strontium substitution on the phase stabilization is less pronounced. No significative change is observed in the β-TCP formation temperature. However, a slight increase of the phase transition temperature is observed for 4.50 mol% of Sr^{2+} and rises a bit with 9.00 mol % (1260 °C and 1270 °C, respectively). So, the strontium substitution allows a slight stabilization of the β-TCP even if it induces an increase of the unit cell parameters due to a higher ionic radius (Fig. 4). Moreover, this stabilization is enhanced with the increasing amount of Sr^{2+} incorporated. This is coherent with results showed by Renaudin et al. [33] where the insertion of Sr^{2+} in the β-TCP structure has clearly a stabilizing effect and improves the geometrical shape of the different cation sites. As explained by the authors, Sr^{2+} cations are preferentially inserted in the Ca(4) site of the β-TCP structure (Fig. 5). In the undoped structure, this site presents a deficiency in the bond valence with three shorter and three larger Ca–O bonds. However, the insertion of strontium in the Ca(4) site modifies its coordination polyhedron leading to six neighboring oxygen atoms with quite equivalent (Ca, Sr)–O bond distances. By consequence, even if the lattice is extended by a Sr^{2+} doping as seen in the XRD results (Figs. 3 and 4), it has a beneficial effect on the bonding forces with oxygen within this lattice leading to a stabilizing effect on the β-TCP structure [33].

3.4. Conventional and microwave sintering of doped β-TCP pellets

Dilatometric results of casted pellets for the different compositions are presented in Fig. 9. Dilatometric curves clearly show different thermal behaviours for all compositions. Undoped β-TCP exhibits a shrinkage of only 2% until the densification is stopped by the volumetric expansion associated to the β→α transition. Indeed, some authors like Frasnelli et al. [14] and Descamps et al. [20] showed that the volumetric
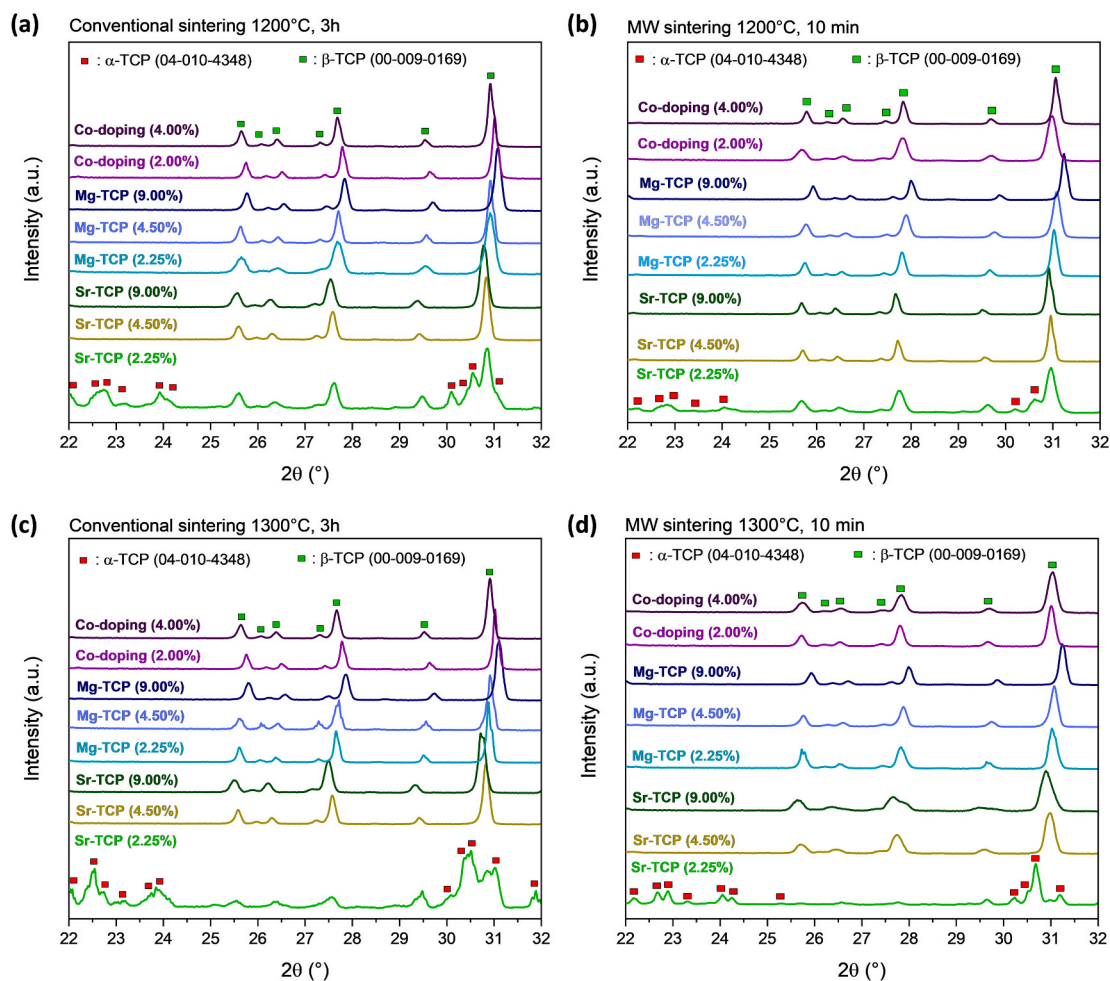
Fig. 11. XRD patterns of conventionally ((a), (c)) and microwave ((b), (d)) sintered doped and co-doped β-TCP pellets at 1200 and 1300 °C.

expansion associated to the β→α transition is visible in dilatometric curves because the densification is suddenly stopped when dilatation occurs. The corresponding phase transition temperature of each composition was thus estimated from these dilatometric curves. These temperatures can be used to classify the stabilization potential of each doping and their ability to postpone the phase transition.

Concerning the doped compositions, a maximum of shrinkage (about 13%) is reached for the 4.50 mol% Mg-TCP while the 9.00 mol% Mg-TCP is already fully dense (99% RD) after the pre-heating treatment at 1000 °C for 12 h. It is confirmed that the sudden interruption of shrinkage associated with the α-TCP formation is postponed for doped and co-doped compositions compared to undoped β-TCP. Only the 2.25 mol% strontium doping does not allow a postponement of this phenomenon. These results confirm the stabilization of the β-TCP phase by the incorporation of both magnesium and strontium in the same way as the previous works by Frasnelli et al. [14] and Cacciotti et al. [80]. Volumetric expansion in Mg-TCP appears at temperatures higher than 1350 °C for 2.25 mol% of Mg^{2+} while it takes place at around 1200 °C for 2.25 mol% of Sr^{2+}. Thus, it is clear that magnesium has a stronger effect than strontium on the stabilization of the β phase for a same doping rate. This is consistent with the assumption made by Tarafder et al. [32] about the phase stability probably caused by the presence of magnesium in co-doped Sr–Mg-TCP. This observed Mg^{2+} stabilization is also consistent with the DTA results and the reduction of lattice parameters.

Consequently, it is possible to compare the stabilization potential of the different dopants obtained by dilatometric and DTA experiments. The β→α transition temperatures observed with dilatometric and DTA

experiments for the different doped powders are compared in Table 3. The main tendencies are observed for both measurements and associated β→α transition temperatures are quite similar for each composition. The higher stabilization effect of magnesium compared to strontium is clearly observed for same doping rates with the two methods. Moreover, the enhancement of the β phase stabilization with the increase of dopants amount is also clearly visible, as predicted in the literature [14,23, 31]. A doping with 2.25 mol% of strontium is not sufficient for a thermal stabilization regarding its behaviour close to undoped TCP. Concerning the two co-doped compositions, the 4.00 mol% co-doping allows a higher β→α transition temperature compare to the 2.00 mol% co-doping in the same way as magnesium and strontium doping tendencies. These values are compared with the literature and previous work about Mg^{2+} doping of Frasnelli et al. [14] and Enderle et al. [23] (Table 3). In the work of Frasnelli et al. [14], β→α transition temperatures were measured with DTA (10 °C/min) in a similar maneer to this study. On the other hand, Enderle et al. [23] used DTA with undoped and 2.00 mol % of Mg^{2+} (5 °C/min) while 4.00 and 8.00 mol% were measured with XRD. For this reason, temperature values can slightly differ from the DTA values in this paper. Nevertheless, β→α transition temperatures obtained in this work are quite consistent with the literature values. Concerning Sr^{2+} doping, no data are available in the literature as its influence on the β-TCP thermal stability had not been evaluated yet.

XRD patterns of conventionally and microwave sintered undoped β-TCP pellets are presented in Fig. 10. For both sintering methods, α-TCP clearly appears from 1200 °C and it is still more present at 1300 °C while β-TCP is the only phase present at 1100 °C. This is consistent with the literature and the usual phase transition temperature of β-TCP (between
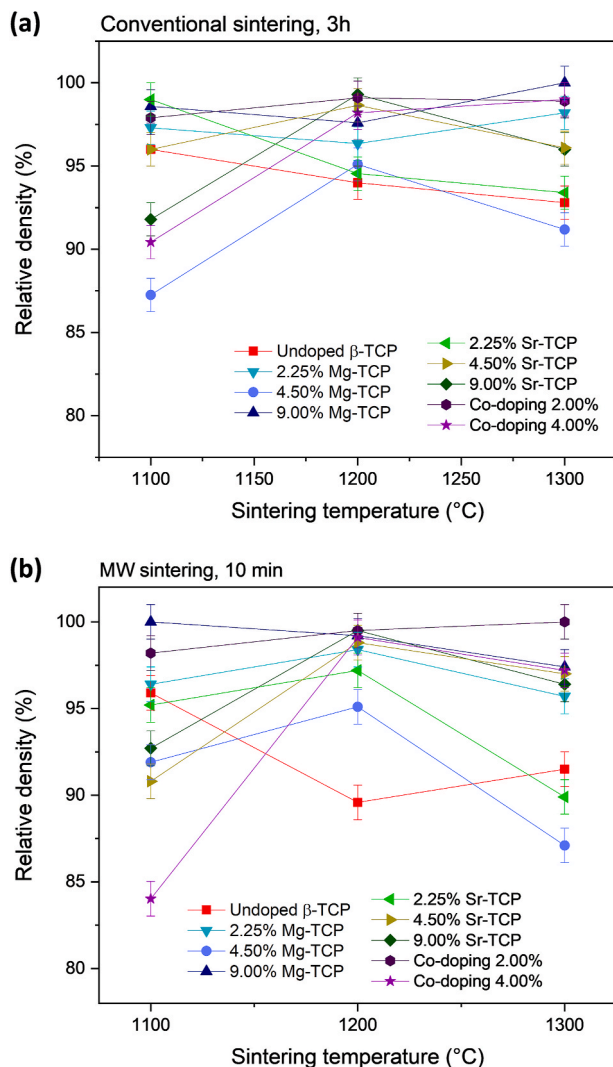
Fig. 12. Relative densities of (a) conventionally and (b) microwave sintered doped and co-doped β-TCP pellets in function of the sintering temperature.

1120 and 1200 °C without dopant).

XRD patterns of doped and co-doped powders are presented in Fig. 11 for conventional ((a) and (c)) and microwave sintering ((b) and (d)) at 1200 and 1300 °C. It appears that the phase stabilization of the β phase by the dopants is achieved up to 1300 °C for all compositions and for both sintering techniques except for the 2.25 mol% Sr-TCP, as expecting from the thermal analyses. Indeed, no characteristic peaks of α-TCP are visible in all concerned XRD patterns. Like doped powders, the two co-doped powders exhibit the same behaviour at high temperatures with an absence of α-TCP and so, a stabilization of the β phase in these conditions. These observations are consistent with the DTA curves and dilatometric results showing that these compositions present postponed transition temperatures (Figs. 8 and 9).

Relative densities of conventionally and microwave sintered pellets are compared in terms of sintering temperature and doping amount in Fig. 12. A clear decrease of density can be observed with the two sintering methods from 1200 °C for some compositions: the undoped β-TCP, the 2.25 mol% Sr-TCP and the 4.50 mol% Mg-TCP. Comparing with the XRD analyses, the decrease of density for the undoped TCP and for the 2.25 mol% Sr-TCP can be attributed to the β→α phase transition. Indeed, α-TCP was found only in these compositions for a sintering at 1300 °C. On the other hand, there is no trace of α-TCP in the diffractograms of 4.50 mol% Mg-TCP. Thus, the β-TCP phase transition does not seem to be the cause of this density drop. This might come from
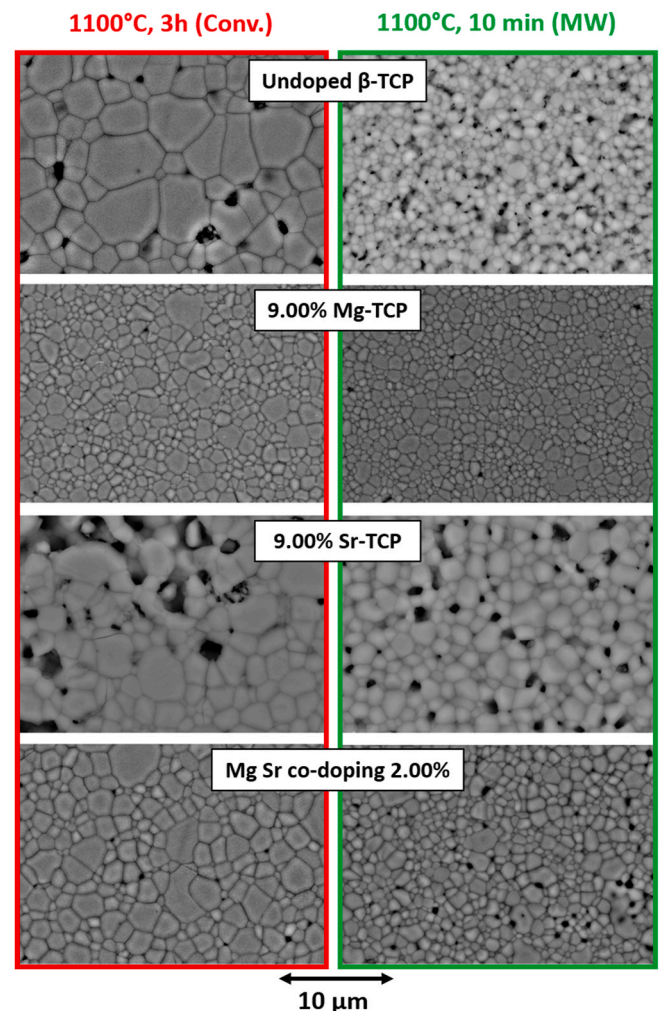

Fig. 13. Micrographs of undoped and doped β-TCP pellets sintered by conventional and microwave sintering.

Table 4
Grain size of conventional and microwave sintered pellets.

Powders	Grain size (μm)	
	1100 °C, 3h (Conv.)	1100 °C, 10 min (MW)
Undoped	2.87 ± 1.68	1.12 ± 0.33
9.00% Mg	1.16 ± 0.50	1.02 ± 0.46
9.00% Sr	2.16 ± 0.87	1.84 ± 0.61
2.00–2.00% Mg–Sr	1.64 ± 0.81	1.12 ± 0.38

the presence of CPP visible in DTA curves in this composition (around 1280 °C in Fig. 8). Indeed, according to Descamps et al. [20] the pyrophosphate phase has a harmful effect on the TCP sinterability. Moreover, the same inconsistency was observed by Ryu et al. [15] in $Ca_2P_2O_7$-doped TCP samples. CPP undergoes a phase transition from the β→α phase around 1220 °C followed by the fusion of the α- $Ca_2P_2O_7$ around 1280 °C [2]. These two phenomena take place in the range in which the decrease of density is observed and can possibly confirm the unfavorable presence of $Ca_2P_2O_7$ on the densification. Nevertheless, higher densities close to 100% can be achieved with the other compositions compared to the undoped β-TCP. Moreover, these relatively high densities remain rather constant even at 1300 °C and all values are quite similar between conventional and microwave sintering. Thus, Mg^{2+} and Sr^{2+} doping can help to sinter β-TCP at higher temperature than the usual phase transition limit without any decrease of density due to this β→α transition.

Microstructures obtained by conventional and microwave sintering are compared in Fig. 13 and in Table 4 with the corresponding average grain sizes. A complete microwave sintering with a dwell time of 10 min at 1200 °C can be carried out in 40 min compared to a conventional sintering (1200 °C, 3 h) of around 10 h. The reduction of the grain size with microwave sintering is clearly visible in the SEM pictures (Fig. 13) and Table 4. Indeed, grain sizes are smaller with microwave sintering for all compositions and it is even halved for the undoped β-TCP compared to conventional sintering. In addition to the reduction of grain size, the microwave sintering also allows a more homogenous grain size distribution regarding the smaller standard deviation compared to conventional sintering (Table 4). Finally, the benefit of the dopants on the grain size is mostly visible with conventional sintering where the grain growth is limited compared to undoped β-TCP.

The microstructures in Fig. 13 confirm the relative densities shown in Fig. 12. Indeed, the 9.00 mol% Mg-TCP possesses the highest densities in both conventional and microwave sintering (98 ± 1% and 99 ± 1% respectively). It is confirmed in the SEM pictures where a clear decrease of the porosity and an enhancement of the densification are observed with the presence of magnesium in the 9.00 mol% Mg-TCP as well in the 2.00 mol% co-doping. The latter is slightly less dense than 9.00 mol% Mg-TCP (97 ± 1% in conventional and 98 ± 1% in microwave) while the undoped β-TCP has relative densities of 94 ± 1% and 96 ± 1% in conventional and microwave sintering, respectively. Finally, the 9.00 mol% Sr-TCP has the lowest densities among the four analyzed compositions (91 ± 1% in conventional and 92 ± 1% in microwave). Its low densification is confirmed in Fig. 13. The incorporation of 9.00 mol% of Sr^{2+} seems to lead to a slowdown in densification until 1100 °C compared to undoped and 9.00 mol% Mg-TCP. Indeed, the presence of numerous large pores in the microstructure and the lower relative densities at 1100 °C after both conventional and microwave sintering confirm this hypothesis. Moreover, the relative densities of the pre-sintered pellets before dilatometry analyses corroborate this slower densification for Sr-TCP. A relative density of 84% was obtained for 9.00 mol% Sr-TCP instead of 85% and 99% for undoped and 9.00 mol% of Mg^{2+}, respectively. However, the Sr-TCP densification seems to be accelerated with the increase of the sintering temperature to 1200 °C to reach almost 100% (Fig. 12). The 2.00 mol% co-doping seems an interesting option with the compromise between an improved densification and a residual porosity useful for tissue reconstruction. This combination of both strontium and magnesium is very promising for bone substitutes from a mechanical and biological point of view as showed by Bose et al. [9,31, 32,64].

4. Conclusion

Eight different compositions of doped β-TCP with magnesium and strontium were successfully synthesized by aqueous precipitation route to increase the thermal stability of the β phase. The powders were fully characterized in terms of composition and thermal behaviour. Infrared spectroscopy, X-ray diffraction, thermal analyses, ICP-AES as well as Rietveld refinements allowed to assess the composition of the produced powders and evaluate the dopants substitution inside the β-TCP structure. A classification of the thermal stabilization potential of the doping was also possible with the strong complementarity of dilatometric and DTA experiments. Indeed, these results highlight the effects of Mg^{2+} and Sr^{2+} dopings on the thermal stability of β-TCP. It has been shown that in all doped compositions, except the 2.25 mol% Sr-TCP, the thermal stability of β-TCP is increased by postponing the β→α transition to higher temperatures. It has also been confirmed that magnesium has a stronger effect than strontium on the stabilization of the β phase for a same doping amount. XRD analyses of sintered pellets showed that the phase stabilization of the β phase by the dopants until 1300 °C is achieved for all compositions except for the 2.25 mol% Sr-TCP with conventional and microwave sintering. Higher densities close to 100% were achieved with the incorporation of dopants compared to the undoped β-TCP. Similar

sintered densities can be obtained with conventional and microwave sintering. However, the thermal process duration is almost sixteen times shorter for microwave sintering allowing a rapid densification without the inconvenient of the β→α transition when dopants are added into the β-TCP structure. The reduction of the grain sizes as well as the more homogenous grain size distributions obtained with microwave sintering are also interesting. Thus, coupling the doping of β-TCP with an alternative sintering method like microwave sintering can be a strong tool to quickly produce dense and stable β-TCP parts. Finally, the use of Sr^{2+} and Mg^{2+} co-doped β-TCP could be very promising for biomedical applications due to the important role of these two cations in biological processes [65].

Declaration of competing interest

The authors declare that they have no known competing financial interests or personal relationships that could have appeared to influence the work reported in this paper.

Acknowledgements

Appendix A. Supplementary data

Supplementary data to this article can be found online at https://doi. org/10.1016/j.oceram.2021.100168.

References

[1] M. Bohner, Bone Substitute Materials, third ed., Elsevier, 2014 https://doi.org/ 10.1016/B978-0-12-801238-3.00224-5.

[2] A. Destainville, E. Champion, E. Laborde, Synthesis, characterization and thermal behavior of apatitic tricalcium phosphate, Mater. Chem. Phys. 80 (2003) 269–277.

[3] S. Bose, S. Vahabzadeh, A. Bandyopadhyay, Bone tissue engineering using 3D printing, Mater. Today 16 (2013) 496–504, https://doi.org/10.1016/j. mattod.2013.11.017.

[4] N. Eliaz, N. Metoki, Calcium phosphate bioceramics: a review of their history, structure, properties, coating technologies and biomedical applications, Materials 10 (2017), https://doi.org/10.3390/ma10040334.

[5] M. Bohner, B.L.G. Santoni, N. Döbelin, β-tricalcium phosphate for bone substitution: synthesis and properties, Acta Biomater. 113 (2020) 23–41, https:// doi.org/10.1016/j.actbio.2020.06.022.

[6] S. Raynaud, E. Champion, D. Bernache-assallant, J. Laval, Determination of calcium/phosphorus atomic ratio of apatites using X-ray diffractometry, J. Am. Ceram. Soc. 84 (2001) 359–366, https://doi.org/10.1111/j.1151-2916.2001. tb00663.x.

[7] W. Habraken, P. Habibovic, M. Epple, M. Bohner, Calcium phosphates in biomedical applications: materials for the future? Mater. Today 19 (2016) 69–87, https://doi.org/10.1016/j.mattod.2015.10.008.

[8] S.V. Dorozhkin, Calcium orthophosphates (CaPO4): occurrence and properties, Am. J. Roentgenol. 160 (1993) 1359, https://doi.org/10.1007/s40204-015-0045-z.

[9] K. Devoe, S. Banerjee, M. Roy, A. Bandyopadhyay, S. Bose, Resorbable tricalcium phosphates for bone tissue engineering: influence of Sro doping, J. Am. Ceram. Soc. 95 (2012) 3095–3102, https://doi.org/10.1111/j.1551-2916.2012.05356.x.

[10] T.N. Aldelaimi, The Use of Resorbable Tricalcium Phosphate Material (β TCP) in Treatment of Surgical Bony Defects after Minor Surgical, 2016.

[11] M. Bohner, Resorbable biomaterials as bone graft substitutes, Mater, Today Off. 13 (2010) 24–30, https://doi.org/10.1016/S1369-7021(10)70014-6.

[12] J. Isaac, J. Hornez, D. Jian, M. Descamps, P. Hardouin, D. Magne, β-TCP microporosity decreases the viability and osteoblast differentiation of human bone marrow stromal cells, J. Biomed. Mater. Res. 86A (2008) 386–393, https://doi. org/10.1002/jbm.a.31644.

[13] S. Bose, S. Tarafder, Calcium phosphate ceramic systems in growth factor and drug delivery for bone tissue engineering: a review, Acta Biomater. 8 (2012) 1401–1421, https://doi.org/10.1016/j.actbio.2011.11.017.

[14] M. Frasnelli, V.M. Sglavo, Effect of Mg2+doping on beta-alpha phase transition in tricalcium phosphate (TCP) bioceramics, Acta Biomater. 33 (2016) 283–289, https://doi.org/10.1016/j.actbio.2016.01.015.

[15] H.S. Ryu, H.J. Youn, K. Sun Hong, B.S. Chang, C.K. Lee, S.S. Chung, An improvement in sintering property of β-tricalcium phosphate by addition of calcium pyrophosphate, Biomaterials 23 (2002) 909–914, https://doi.org/10.1016/S0142-9612(01)00201-0.

[16] W.Y. Wong, A.F. Mohd Noor, R. Othman, Sintering of beta-tricalcium phosphate scaffold using polyurethane template, Key Eng. Mater. 694 (2016) 94–98. https://doi.org/10.4028/www.scientific.net/kem.694.94.

[17] R. Ghosh, R. Sarkar, Synthesis and characterization of sintered beta-tricalcium phosphate: a comparative study on the effect of preparation route, Mater. Sci. Eng. C 67 (2016) 345–352, https://doi.org/10.1016/j.msec.2016.05.029.

[18] P. Feng, P. Wei, C. Shuai, S. Peng, Characterization of mechanical and biological properties of 3-D scaffolds reinforced with zinc oxide for bone tissue engineering, PloS One 9 (2014), https://doi.org/10.1371/journal.pone.0087755.

[19] M. Sayer, a.D. Stratilatov, J. Reid, L. Calderin, M.J. Stott, X. Yin, M. MacKenzie, T. J.N. Smith, J.a. Hendry, S.D. Langstaff, Structure and composition of silicon-stabilized tricalcium phosphate, Biomaterials 24 (2003) 369–382, https://doi.org/10.1016/S0142-9612(02)00327-7.

[20] M. Descamps, J.C. Hornez, a. Leriche, Effects of powder stoichiometry on the sintering of β-tricalcium phosphate, J. Eur. Ceram. Soc. 27 (2007) 2401–2406, https://doi.org/10.1016/j.jeurceramsoc.2006.09.005.

[21] P. Hudon, I.H. Jung, Critical evaluation and thermodynamic optimization of the CaO-P2O5 system, Metall. Mater. Trans. B Process Metall. Mater. Process. Sci. 46 (2015) 494–522, https://doi.org/10.1007/s11663-014-0193-x.

[22] E. Champion, Sintering of calcium phosphate bioceramics, Acta Biomater. 9 (2013) 5855–5875, https://doi.org/10.1016/j.actbio.2012.11.029.

[23] R. Enderle, F. Götz-Neunhoeffer, M. Göbbels, F.a. Müller, P. Greil, Influence of magnesium doping on the phase transformation temperature of β-TCP ceramics examined by Rietveld refinement, Biomaterials 26 (2005) 3379–3384, https://doi.org/10.1016/j.biomaterials.2004.09.017.

[24] R.G. Carrodeguas, A.H. De Aza, X. Turrillas, P. Pena, S. De Aza, New approach to the β→α polymorphic transformation in magnesium-substituted tricalcium phosphate and its practical implications, J. Am. Ceram. Soc. 91 (2008) 1281–1286, https://doi.org/10.1111/j.1551-2916.2008.02294.x.

[25] P.M.C. Torres, J.C.C. Abrantes, A. Kaushal, S. Pina, N. Döbelin, M. Bohner, J.M. F. Ferreira, Journal of the European Ceramic Society Influence of Mg-doping , calcium pyrophosphate impurities and cooling rate on the allotropic _ ↔ ′′ -tricalcium phosphate phase transformations 36 (2016) 817–827.

[26] N. Matsumoto, K. Yoshida, K. Hashimoto, Y. Toda, Thermal stability of β-tricalcium phosphate doped with monovalent metal ions, Mater. Res. Bull. 44 (2009) 1889–1894, https://doi.org/10.1016/j.materresbull.2009.05.012.

[27] R.G. Carrodeguas, S. De Aza, α-Tricalcium phosphate: synthesis, properties and biomedical applications, Acta Biomater. 7 (2011) 3536–3546, https://doi.org/10.1016/j.actbio.2011.06.019.

[28] M. Lasgorceix, C. Ott, L. Boilet, S. Hocquet, A. Leriche, M. Asadian, N. De Geyter, H. Declercq, V. Lardot, F. Cambier, Micropatterning of beta tricalcium phosphate bioceramic surfaces, by femtosecond laser, for bone marrow stem cells behavior assessment, Mater. Sci. Eng. C 95 (2019) 371–380, https://doi.org/10.1016/j.msec.2018.03.004.

[29] Y. Tian, T. Lu, F. He, Y. Xu, H. Shi, X. Shi, F. Zuo, S. Wu, J. Ye, B-tricalcium phosphate composite ceramics with high compressive strength, enhanced osteogenesis and inhibited osteoclastic activities, Colloids Surf. B Biointerfaces 167 (2018) 318–327, https://doi.org/10.1016/j.colsurfb.2018.04.028.

[30] W. Acchar, E.G. Ramalho, Effect of MnO2 addition on sintering behavior of tricalcium phosphate: preliminary results, Mater. Sci. Eng. C 28 (2008) 248–252, https://doi.org/10.1016/j.msec.2006.12.011.

[31] S.S. Banerjee, S. Tarafder, N.M. Davies, A. Bandyopadhyay, S. Bose, Understanding the influence of MgO and SrO binary doping on the mechanical and biological properties of β-TCP ceramics, Acta Biomater. 6 (2010) 4167–4174, https://doi.org/10.1016/j.actbio.2010.05.012.

[32] S. Tarafder, W.S. Dernell, A. Bandyopadhyay, S. Bose, SrO- and MgO-doped microwave sintered 3D printed tricalcium phosphate scaffolds: mechanical properties and in vivo osteogenesis in a rabbit model, J. Biomed. Mater. Res. B Appl. Biomater. 103 (2015) 679–690, https://doi.org/10.1002/jbm.b.33239.

[33] G. Renaudin, E. Jallot, J.M. Nedelec, Effect of strontium substitution on the composition and microstructure of sol-gel derived calcium phosphates, J. Sol. Gel Sci. Technol. 51 (2009) 287–294, https://doi.org/10.1007/s10971-008-1854-5.

[34] E.A. dos Santos, K. Anselme, G.D. de Almeida Soares, A. Kuznetsov, L.Á. de Sena, M.P. Moreira, J. Dentzer, Synthesis of magnesium- and manganese-doped hydroxyapatite structures assisted by the simultaneous incorporation of strontium, Mater. Sci. Eng. C 61 (2016) 736–743, https://doi.org/10.1016/j.msec.2016.01.004.

[35] A. Chanda, S. Dasgupta, S. Bose, A. Bandyopadhyay, Microwave sintering of calcium phosphate ceramics, Mater. Sci. Eng. C 29 (2009) 1144–1149, https://doi.org/10.1016/j.msec.2008.09.008.

[36] H.S. Ryu, K.S. Hong, J.K. Lee, D.J. Kim, J.H. Lee, B.S. Chang, D.H. Lee, C.K. Lee, S. S. Chung, Magnesia-doped HA/β-TCP ceramics and evaluation of their biocompatibility, Biomaterials 25 (2004) 393–401, https://doi.org/10.1016/S0142-9612(03)00538-6.

[37] K.C. Kai, C.a.V.a. Machado, L.A. Genova, J. Marchi, Influence of Zn and Mg doping on the sintering behavior and phase transformation of tricalcium phosphate based ceramics, Mater. Sci. Forum 805 (2014) 706–711. https://doi.org/10.4028/www.scientific.net/MSF.805.706.

[38] L. Obadia, P. Deniard, B. Alonso, T. Rouillon, S. Jobic, J. Guicheux, M. Julien, D. Massiot, B. Bujoli, J.M. Bouler, Effect of sodium doping in β-tricalcium phosphate on its structure and properties, Chem. Mater. 18 (2006) 1425–1433, https://doi.org/10.1021/cm052135f.

[39] K. Prem Ananth, S. Shanmugam, S.P. Jose, a. Joseph Nathanael, T.H. Oh, D. Mangalaraj, A.M. Ballamurugan, Structural and chemical analysis of silica-doped β-TCP ceramic coatings on surgical grade 316L SS for possible biomedical application, J. Asian Ceram. Soc. 3 (2015) 317–324, https://doi.org/10.1016/j.jascer.2015.06.004.

[40] S. Gomes, C. Vichery, S. Descamps, H. Martinez, A. Kaur, A. Jacobs, J.M. Nedelec, G. Renaudin, Cu-doping of calcium phosphate bioceramics: from mechanism to the control of cytotoxicity, Acta Biomater. 65 (2018) 462–474, https://doi.org/10.1016/j.actbio.2017.10.028.

[41] A. Bioactive, G. Bone, M.M. Ferreira, A.F. Brito, D. Brazete, C. Pereira, E. Carrilho, A.M. Abrantes, A.S. Pires, M.J. Aguiar, L. Carvalho, M.F. Botelho, J.M.F. Ferreira, Doping β -TCP as a Strategy for Enhancing the Regenerative Potential of Composite Experimental Study in Rats, 2019, https://doi.org/10.3390/ma12010004.

[42] G. Li, N. Zhang, S. Zhao, K. Zhang, X. Li, A. Jing, X. Liu, T. Zhang, Fe-doped brushite bone cements with antibacterial property, Mater. Lett. 215 (2018) 27–30, https://doi.org/10.1016/j.matlet.2017.12.054.

[43] I.V. Fadeeva, M.R. Gafurov, I.A. Kiiaeva, S.B. Orlinskii, L.M. Kuznetsova, Y. Y. Filippov, A.S. Fomin, G.A. Davydova, I.I. Selezneva, S.M. Barinov, Tricalcium phosphate ceramics doped with silver, copper, zinc, and iron (III) ions in concentrations of less than 0.5 wt.% for bone tissue regeneration, Bionanoscience 7 (2017) 434–438, https://doi.org/10.1007/s12668-016-0386-7.

[44] Z.Y. Qiu, G. Li, Y.Q. Zhang, J. Liu, W. Hu, J. Ma, S.M. Zhang, Fine structure analysis and sintering properties of Si-doped hydroxyapatite, Biomed. Mater. 7 (2012), https://doi.org/10.1088/1748-6041/7/4/045009.

[45] R. Sasidharan Pillai, V.M. Sglavo, Effect of MgO addition on solid state synthesis and thermal behavior of beta-tricalcium phosphate, Ceram. Int. 41 (2015) 2512–2518, https://doi.org/10.1016/j.ceramint.2014.10.073.

[46] X. Wei, M. Akinc, Crystal structure analysis of Si- and Zn-codoped tricalcium phosphate by neutron powder diffraction, J. Am. Ceram. Soc. 90 (2007) 2709–2715, https://doi.org/10.1111/j.1551-2916.2007.01764.x.

[47] S. Bose, S. Tarafder, S.S. Banerjee, N.M. Davies, A. Bandyopadhyay, Understanding in vivo response and mechanical property variation in MgO, SrO and SiO2 doped β-TCP, Bone 48 (2011) 1282–1290, https://doi.org/10.1016/j.bone.2011.03.685.

[48] G.a. Fielding, A. Bandyopadhyay, S. Bose, Effects of silica and zinc oxide doping on mechanical and biological properties of 3D printed tricalcium phosphate tissue engineering scaffolds, Dent. Mater. 28 (2012) 113–122, https://doi.org/10.1016/j.dental.2011.09.010.

[49] G. Renaudin, S. Gomes, J.M. Nedelec, First-row transition metal doping in calcium phosphate bioceramics: a detailed crystallographic study, Materials 10 (2017) 1–22, https://doi.org/10.3390/ma10010092.

[50] P.M.C. Torres, S.I. Vieira, a.R. Cerqueira, S. Pina, O.a.B. Da Cruz Silva, J.C. C. Abrantes, J.M.F. Ferreira, Effects of Mn-doping on the structure and biological properties of β-tricalcium phosphate, J. Inorg. Biochem. 136 (2014) 57–66, https://doi.org/10.1016/j.jinorgbio.2014.03.013.

[51] K. Yoshida, H. Hyuga, N. Kondo, H. Kita, M. Sasaki, M. Mitamura, K. Hashimoto, Y. Toda, Substitution model of monovalent (Li, Na, and K), divalent (Mg), and trivalent (Al) metal ions for β-tricalcium phosphate, J. Am. Ceram. Soc. 89 (2006) 688–690, https://doi.org/10.1111/j.1551-2916.2005.00727.x.

[52] D.J. Curran, T.J. Fleming, M.R. Towler, S. Hampshire, Mechanical parameters of strontium doped hydroxyapatite sintered using microwave and conventional methods, J. Mech. Behav. Biomed. Mater. 4 (2011) 2063–2073, https://doi.org/10.1016/j.jmbbm.2011.07.005.

[53] F. Zhang, K. Lin, J. Chang, J. Lu, C. Ning, Spark plasma sintering of macroporous calcium phosphate scaffolds from nanocrystalline powders, J. Eur. Ceram. Soc. 28 (2008) 539–545, https://doi.org/10.1016/j.jeurceramsoc.2007.07.012.

[54] L. Boilet, M. Descamps, E. Rguiti, A. Tricoteaux, J. Lu, F. Petit, V. Lardot, F. Cambier, A. Leriche, Processing and properties of transparent hydroxyapatite and β tricalcium phosphate obtained by HIP process, Ceram. Int. 39 (2013) 283–288, https://doi.org/10.1016/j.ceramint.2012.06.023.

[55] S. Tarafder, , S., V.K. Balla, N.M. Davies, A. Bandyopadhyay, Bose, Microwave-sintered 3D printed tricalcium phosphate scaffolds for bone tissue engineering, J. Tissue Eng. Regen. Med. 13 (2012) 512–520, https://doi.org/10.1002/term.

[56] A. Leriche, E. Savary, A. Thuault, J.-C. Hornez, M. Descamps, S. Marinel, Comparison of conventional and microwave sintering of bioceramics, Adv. Process. Manuf. Technol. Nanostructured Multifunct. Mater. (2015) 23–32, https://doi.org/10.1002/9781119040354.ch3.

[57] M. Casas-Luna, H. Tan, S. Tkachenko, D. Salamon, E.B. Montufar, Enhancement of mechanical properties of 3D-plotted tricalcium phosphate scaffolds by rapid sintering, J. Eur. Ceram. Soc. 39 (2019) 4366–4374, https://doi.org/10.1016/j.jeurceramsoc.2019.05.055.

[58] H. Curto, A. Thuault, F. Jean, M. Violier, V. Dupont, J.-C. Hornez, A. Leriche, Coupling additive manufacturing and microwave sintering: a fast processing route of alumina ceramics, J. Eur. Ceram. Soc. (2019) 1, https://doi.org/10.1016/j.jeurceramsoc.2019.11.009.

[59] Trunec Martin, Effect of grain size on mechanical properties of full-dense Pb(Zr,Ti) O 3 ceramics, Jpn. J. Appl. Phys. 49 (2010) 1–8, https://doi.org/10.1143/JJAP.49.09MD13.

[60] A. Thuault, E. Savary, J.C. Hornez, G. Moreau, M. Descamps, S. Marinel, A. Leriche, Improvement of the hydroxyapatite mechanical properties by direct microwave sintering in single mode cavity, J. Eur. Ceram. Soc. 34 (2014) 1865–1871, https://doi.org/10.1016/j.jeurceramsoc.2013.12.035.

[61] S. Dasgupta, S. Tarafder, A. Bandyopadhyay, S. Bose, Effect of grain size on mechanical, surface and biological properties of microwave sintered hydroxyapatite, Mater. Sci. Eng. C 33 (2013) 2846–2854, https://doi.org/10.1016/j.msec.2013.03.004.

[62] E. Savary, A. Thuault, J.-C. Hornez, M. Descamps, S. Marinel, A. Leriche, Frittage micro-ondes en cavité monomode de biocéramiques, MATEC Web Conf 7 (2013), 04017, https://doi.org/10.1051/matecconf/20130704017.

[63] G.A. Kriegsmann, Thermal runaway in microwave heated ceramics: a one-dimensional model, J. Appl. Phys. 71 (1992) 1960–1966, https://doi.org/10.1063/1.351191.

[64] S. Bose, G. Fielding, S. Tarafder, A. Bandyopadhyay, Understanding of dopant-induced osteogenesis and angiogenesis in calcium phosphate ceramics, Trends Biotechnol. 31 (2013) 594–605, https://doi.org/10.1016/j.tibtech.2013.06.005.

[65] S. Kannan, F. Goetz-Neunhoeffer, J. Neubauer, S. Pina, P.M.C. Torres, J.M. F. Ferreira, Synthesis and structural characterization of strontium- and magnesium-co-substituted β-tricalcium phosphate, Acta Biomater. 6 (2010) 571–576, https://doi.org/10.1016/j.actbio.2009.08.009.

[66] S.S. Banerjee, A. Bandyopadhyay, S. Bose, Biphasic resorbable calcium phosphate ceramic for bone implants and local alendronate delivery, Adv. Eng. Mater. 12 (2010) 148–155, https://doi.org/10.1002/adem.200980072.

[67] D. Veljovic, Z. Radovanovic, A. Dindune, E. Palcevskis, A. Krumina, R. Petrovic, D. Janackovic, The influence of Sr and Mn incorporated ions on the properties of microwave single- and two-step sintered biphasic HAP/TCP bioceramics, J. Mater. Sci. 49 (2014) 6793–6802, https://doi.org/10.1007/s10853-014-8380-3.

[68] D. Ke, S. Bose, Doped tricalcium phosphate bone tissue engineering scaffolds using sucrose as template and microwave sintering: enhancement of mechanical and biological properties, Mater. Sci. Eng. C 78 (2017) 398–404, https://doi.org/10.1016/j.msec.2017.03.167.

[69] R.K. Chadha, K.L. Singh, C. Sharma, A.P. Singh, V. Naithani, Effect of microwave and conventional processing techniques on mechanical properties of Strontium substituted hydroxyapatite, Ceram. Int. 46 (2020) 1091–1098, https://doi.org/10.1016/j.ceramint.2019.09.076.

[70] K. Matsunaga, T. Kubota, K. Toyoura, A. Nakamura, First-principles calculations of divalent substitution of Ca^{2+} in tricalcium phosphates, Acta Biomater. 23 (2015) 329–337, https://doi.org/10.1016/j.actbio.2015.05.014.

[71] B. Bracci, P. Torricelli, S. Panzavolta, E. Boanini, R. Giardino, a. Bigi, Effect of Mg2+, Sr2+, and Mn2+ on the chemico-physical and in vitro biological properties of calcium phosphate biomimetic coatings, J. Inorg. Biochem. 103 (2009) 1666–1674, https://doi.org/10.1016/j.jinorgbio.2009.09.009.

[72] S. Chamary, Influence de l ' architecture macroporeuse en phosphate de calcium sur le comportement cellulaire in vitro To cite this version : HAL Id : tel-01822768, Université de Valenciennes et du Hainaut-Cambrésis, 2018.

[73] A. Thuault, S. Marinel, E. Savary, R. Heuguet, S. Saunier, D. Goeuriot, D. Agrawal, Processing of reaction-bonded B4C–SiC composites in a single-mode microwave cavity, Ceram. Int. 39 (2013) 1215–1219, https://doi.org/10.1016/J.CERAMINT.2012.07.047.

[74] N. Doebelin, R. Kleeberg, Computer Programs Profex : a Graphical User Interface for the Rietveld Refinement Program BGMN, 2015, pp. 1573–1580, https://doi.org/10.1107/S1600576715014685.

[75] M. Abercrombie, Estimation of nuclear population from microtome sections, Anat. Rec. 94 (1946) 239–247.

[76] A.R. Denton, N.W. Ashcroft, Vegards law, Phys. Rev. 43 (1991) 3161–3164, https://doi.org/10.1103/PhysRevA.43.3161.

[77] E. Boanini, M. Gazzano, C. Nervi, M.R. Chierotti, K. Rubini, R. Gobetto, A. Bigi, Strontium and zinc substitution in β-tricalcium phosphate: an X-ray diffraction, solid state NMR and ATR-FTIR study, J. Funct. Biomater. 10 (2019), https://doi.org/10.3390/jfb10020020.

[78] B. Le Gars Santoni, L. Niggli, G.A. Sblendorio, D.T.L. Alexander, C. Stahli, P. Bowen, N. Dobelin, M. Bohner, Chemically pure β-tricalcium phosphate powders: evidence of two crystal structures, J. Eur. Ceram. Soc. 41 (2021) 1683–1694, https://doi.org/10.1016/j.jeurceramsoc.2020.09.055.

[79] A. Mortier, J. Lemaitre, P.G. Rouxhet, Temperature-programmed characterization of synthetic calcium-deficient phosphate apatites, Thermochim. Acta 143 (1989) 265–282, https://doi.org/10.1016/0040-6031(89)85065-8.

[80] I. Cacciotti, A. Bianco, High thermally stable Mg-substituted tricalcium phosphate via precipitation, Ceram. Int. 37 (2011) 127–137, https://doi.org/10.1016/j.ceramint.2010.08.023.